IOP Conf. Series: Materials Science and Engineering **454** (2018) 012040 doi:10.1088/1757-899X/454/1/012040

Effect of thermomechanical processing and heat treatment on the microstructure evolution of the Ti-6246 alloy

Mohammed H Alluaibi[1,2] and Vasile D Cojocaru[1]

[1]Faculty of Material Science and Engineering, University POLITEHNICA of Bucharest, Romania
[2]Corresponding author. E-mail address: mohammed.aluaibi@gmail.com

Abstract. In the present study, the microstructures of five samples of the Ti-6246 alloy were investigated using SEM and OM devices. Four samples had been examined during different thermo-mechanical processing and heat treatment (hot plastic deformation and normalizing heat treatment) in α + β and β field domain respectively. The results demonstrate that the phase transformations and compositional modifications induced by thermo-mechanical processing and heat treatment have a dramatic influence on the microstructural characteristics. It was concluded that all samples present many morphologies textures and orientations. The microstructures features had improved in the normalizing heat process in comparison with the parent material and the hot deformation process.

Keywords: Titanium alloys, microstructure, thermomechanical processing, heat treatment

1. Introduction

Over the past six decades, the titanium (Ti) based alloys have attracted the attention of the authors and the researchers because it possess unique properties that make it distinct from other alloys. Various types of Ti-based alloys are available, the Ti-6Al-2Sn-4Zr-6Mo (Ti-6246) alloy is one of the most popular alloys was developed by Pratt and Whitney (P&W) in the United States around 1966 to provide high strength alloy. The alloy is widely used in aero-engine components because it has important features such as low density, high strength, and excellent corrosion resistance to the high extreme environment [1, 2, 3]. On the other hand, the most flaws of this alloy are the high cost and the difficulty of extraction and separation of raw materials in spite of many attempts, even nowadays, these obstacles still exist. Titanium alloys can be categorized as α + β titanium alloys group from the alloying elements partitioning viewpoint. α + β alloys are rich of both α and β stabilizers, comprising around 4 to 6% of β stabilizers which make them very desirable to develop high strength alloys. Near-β or "metastable β" alloys have less amount relatively of β-stabilizers that contains approximately (10% - 15%) in comparison with β alloys includes large quantities of β-stabilizers (around 30%) that stabilize β phase at an ambient temperature which is considered the very heavily β-stabilized alloys. On the contrary, Ti-alloys type α is single phase alloys i.e. they do not have β-stabilizers elements and near-α/super α alloys have a slightly higher response to the thermo-mechanical processes (TMPs) than α alloys. This is because they contain a slight percentage (up to 2 wt. %) of β-stabilizer leads to enhance their workability, ductility, and strength [4, 5, 6].

Earlier, Boyer [1] has reported that Ti-6246 alloy used essentially in the military aircraft engines like F-I00 and F-119 at a yield stress scale of 1035 MPa, but the properties of damage tolerance for this alloy are not good in comparison with Ti-6Al-4V and Ti-6Al-2Sn-4Zr-2Mo alloys. Therefore, the Ti-6246 alloy is not used in commercial engines due to the shorter examination periods that would be

required. Ti-6246 alloy has a low possibility in taking place the essential imperfections like the gas porosity which exist as a result of the melting or/and the inclusions of ceramic that may occur normally in industrial alloys. Moreover, this property makes it more attractive in many methods of static applications in the chemical processes and aerospace industries [7, 8, 9].

Recently, Pretorius et al. [10] have stated that around 33% of the weight of a civilian aircraft engines is made up of titanium alloys, whereas was about 50% for the military aero-engines. On the other hand, Pederson et al. [11] they have mentioned that Ti-6246 alloy is appreciated for the aerospace industry such as fans and compressor rotors parts which required high loads at intermediate temperatures. Furthermore, some applications of the Ti-6246 alloy at medium temperatures like jet engine components, the inner part in gas turbine discs and impellers, in the deep sour well components, also used as a part of the blades, disc, and seal [7, 10].

The β-transus temperature (TT_β) is a central point in the thermo-mechanical processing topic because it is working to an arrangement and separate of the alpha and beta phases [12]. It can be defined as the lowest equilibrium temperature at which the material is 100% β [13, 14]. Several attempts have been conducted to explore the influence of (TMPs) and heat treatments (HTs) on the microstructure and mechanical properties of α + β titanium alloys to produce maximum strengths alloys [15-19]. Generally, α + β alloys required a combination of TMPs and HTs to change the microstructures and mechanical characteristics in comparison with β alloys that can be changed dramatically just by HTs [20-22].

The titanium alloys underwent to the thermo-mechanical processes which affected dramatically in accordance with the different temperatures used and the type of the thermo-mechanical process applied to the alloy. The main purpose of the thermo-mechanical processes of titanium alloys is to create the forms required for use through the primary work (ingot breakdown) and then set it up for the secondary work (mill operations) such as hot rolling or forging for example. Besides, to improve the mechanical properties by the control the microstructure during apply different stages of thermo-mechanical processes [23, 24]. The main objective of the present paper is to examine the changes in the microstructures development during different steps of TMP and HT.

2. Materials and Methods

The workpiece material is Ti-6246 alloy as-cast was chosen for this paper which has TT_β 940ºC ±5ºC [14, 25-27]. This alloy obtained by Vacuum Arc Remelting (VAR) at Zirom S.A. of Giurgiu, Romania. Table 1 shows the chemical composition of Ti-6246 alloy (as-cast).

Table 1. The chemical composition of the Ti-6246 alloy as-cast.

Alloy type	Components of alloy (wt. %)					
Ti-6246	Al (5.50)	Sn (1.34)	Zr (3.60)	Mo (5.96)	Fe (0.06)	Ti (Balance)

The samples that have been prepared from the as-cast alloy were cut into two parts by using a precision cutter device model Metkon Micracut 200. The dimension of these parts before deformation was around 27 mm, 11 mm and 4.2 mm. Five samples were investigated for the microstructures of Ti-6246 alloy; sample I (as-cast), samples II and IV were examined for hot plastic deformation process at temperatures lower than Tβ up to 800°C and 900°C respectively. Alongside, samples III and V were inspected to the normalizing heat treatment with a stable temperature slightly higher than Tβ at 950°C.

Two stages were used to process this alloy, the first one is the TMP includes the samples II and IV that carried out through upsetting (forging) for the alloy with same potential energy (weight) 117 Kg and free fall distance (high) 1m to obtain a higher degree of distortion with maintaining the microstructural integrity throughout the alloy. This process involves deformation below TTβ of the Ti-6246 alloy at temperatures of 800ºC and 900ºC (time duration, 15 mins) and directly cooled at room temperature. The last process is normalizing HT contains the samples III and V which performed at

constant temperature 950°C (time duration, 30 mins), and immediately furnace cooling conditions to ensure sufficiently slow cooling rate for finalizing the microstructure deformation. Figure 1 shows the TMP route used for Ti-6246 alloy.

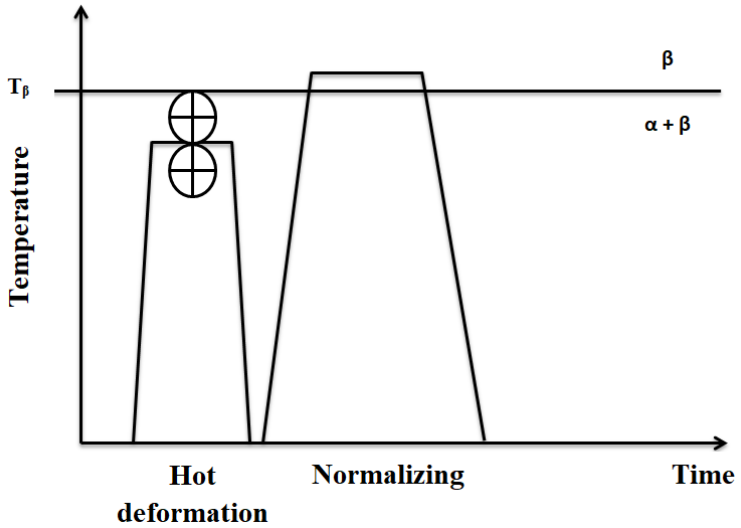

Figure 1. The TMPs route of the Ti-6246 alloy.

Three microstructures have been investigated, as-cast, deformed and normalized samples. Five samples were cut and prepared with a very good surface finish using a precision cutter Metkon Micracut 200. Thereafter, all samples were subjected hot-mounted using a Buehler SimpliMet mounting press inside the cylindrical sampler. Thence, all samples underwent to grinding and polishing using a Metkon DIGIPREP Accura (advanced high-end grinding and polishing system). Eventually, the microstructure was analyzed using scanning electron microscopy (SEM) device model TESCAN VEGA II–XMU and optical microscopy (OM) respectively.

3. Results and Discussions

The samples dimensions II and IV have changed after hot plastic deformation process. Table 2 displays the dimensions of samples II and IV after hot plastic deformation process.

Table 2. The dimensions of samples II and IV after hot deformation process.

New dimensions, (mm)	Samples	
	Sample II	Sample IV
Length	34.4	35.3
Width	22.4	23.4
Thickness	1.8	1.7

The following relation has been used to calculate the deformation degree of samples II and IV:

$$\varepsilon = \frac{H-h}{H}\ 100 \quad (1)$$

Where,
ε - Is the deformation degree (%);
H - Is the initial thickness in (mm);
h - Is the final thickness in (mm).

The deformation degree of samples II and IV were 56.1% and 59.5% respectively. It is worth mentioning that the temperature is proportional directly to the deformation degree, where confirm that the higher the temperature the greater the degree of deformation.

3.1. Alloying elements dispersion

The results of each sample for SEM-BSE and alloying elements dispersion inside the microstructures are shown in Figures 2 - 6. Once seeing SEM-BSE images that are shown in Figures 2a, 3a, 4a, 5a and 6a, the microstructures can be designated. The microstructure that is shown in Figure 2a comprising α-lamellar colonies which have independently adapted in different directions with β-phase dispersed between α-lamellar whereas, the microstructure that shown in Figure 3a includes thick α lamellar among β phase matrix in addition to α lamellar colonies dispersed within the same β phase matrix. Moreover, Figure 4a shows that the microstructure contains α + β lamellar aligned similarly as in the as-cast material while the microstructure in Figure 5a involves crooked α lamellar into β phase matrix. Furthermore, the microstructure inside SEM-BSE image (Figure 6a) is α + β acicular lamellar.

On the other hand, to compute the concentration/content for all alloying elements dispersion, six random microstructural images were obtained and EDS analyzed. Table 3 reveals the results of chemical composition data that were statistically estimated for each sample from the as-cast to V sample. It can be seen that the higher concentration of Ti element is detected in α phase as illustrating in Figures 2b-6b; also Al element as depicted in Figures 2c-6c is considered as α-stabilizer because it has an obvious influence on α-Ti phase. Besides, the Mo and Fe elements as shown in Figures from 2d, 2g to 6d, 6g were identified as β-stabilizer because they work on promotes β-Ti phase. Normally both of Zr and Sn elements have a neutral behavior on two phases of Ti (Figures 2e-6e and Figures 2f-6f), but it was observed Zr element has a strong effect on the β phase by contrast with Sn element that exhibits a moderate dispersion of both phases, except (Figure 5f), it seems to strengthen α-Ti phase more than β phase. As noted in Figures 2h – 6h, the existence of Ti, Al, Mo, Zr, Sn and Fe elements, and there are no other relevant EDS lines being observed [4, 23, 28].

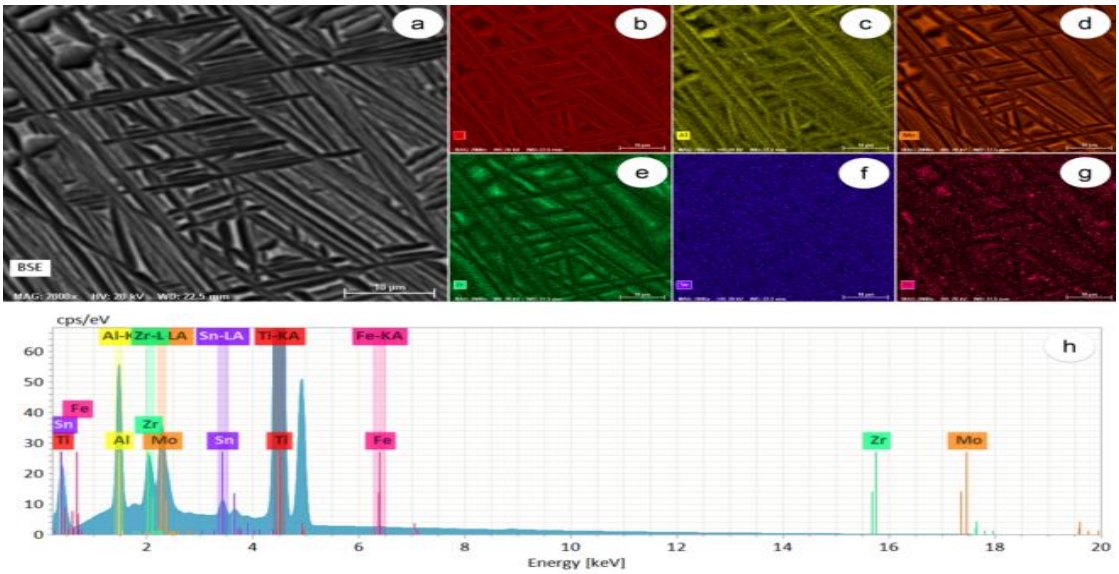

Figure 2. Alloying elements dispersion inside as-cast sample; a) high magnification BSE image of as-cast sample microstructure; b) Ti dispersion; c) Al dispersion; d) Mo dispersion; e) Zr dispersion; f) Sn dispersion; g) Fe dispersion; h) EDS spectra of the as-cast sample.

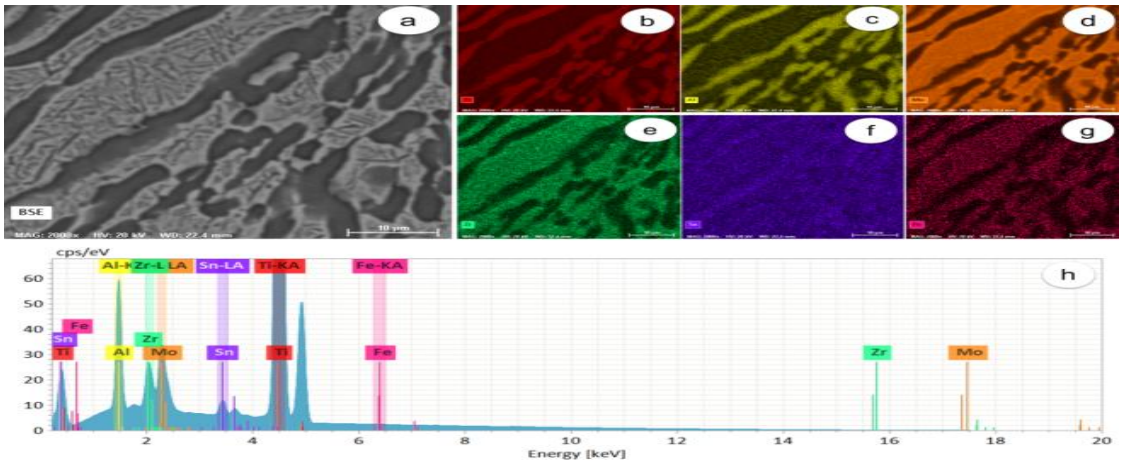

Figure 3. Alloying elements dispersion within the sample II (hot-deformed at 800°C); a) high magnification BSE image of sample II microstructure; b) Ti dispersion; c) Al dispersion; d) Mo dispersion; e) Zr dispersion; f) Sn dispersion; g) Fe dispersion; h) EDS spectra of sample II.

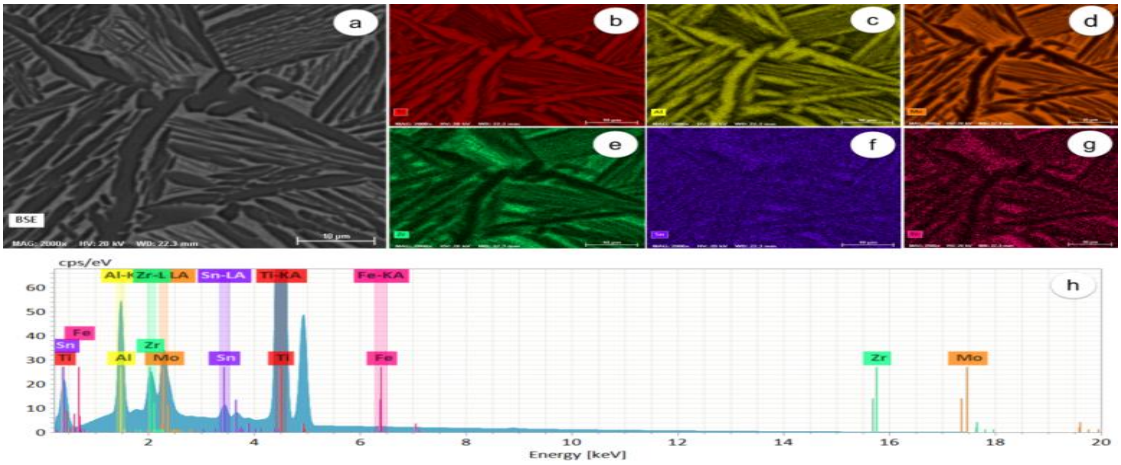

Figure 4. Alloying elements dispersion inside the sample III (hot-deformed at 800°C and normalized at 950°C); a) high magnification BSE image of sample III microstructure; b) Ti dispersion; c) Al dispersion; d) Mo dispersion; e) Zr dispersion; f) Sn dispersion; g) Fe dispersion; h) EDS spectra of sample III.

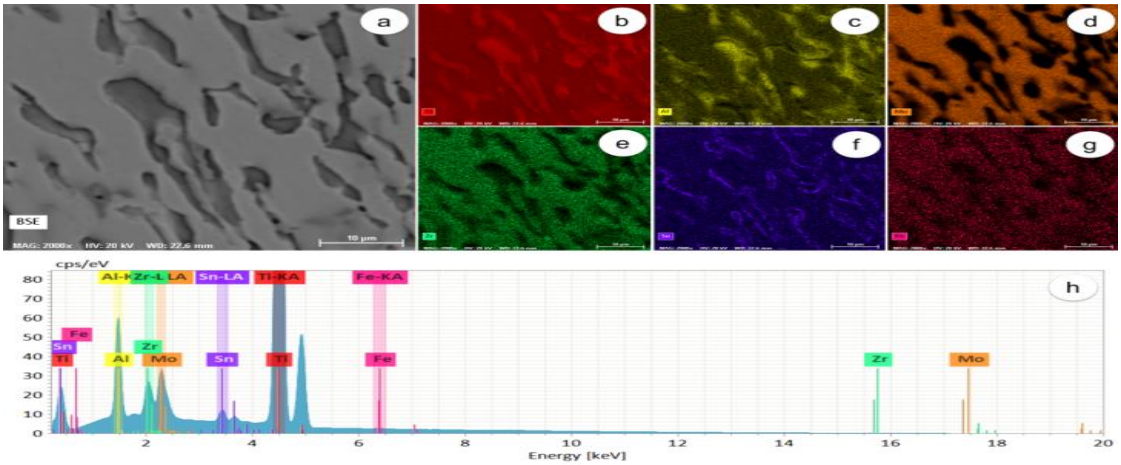

Figure 5. Alloying elements dispersion into the sample IV (hot-deformed at 900°C); a) high magnification BSE image of sample IV microstructure; b) Ti dispersion; c) Al dispersion; d) Mo dispersion; e) Zr dispersion; f) Sn dispersion; g) Fe dispersion; h) EDS spectra of sample IV.

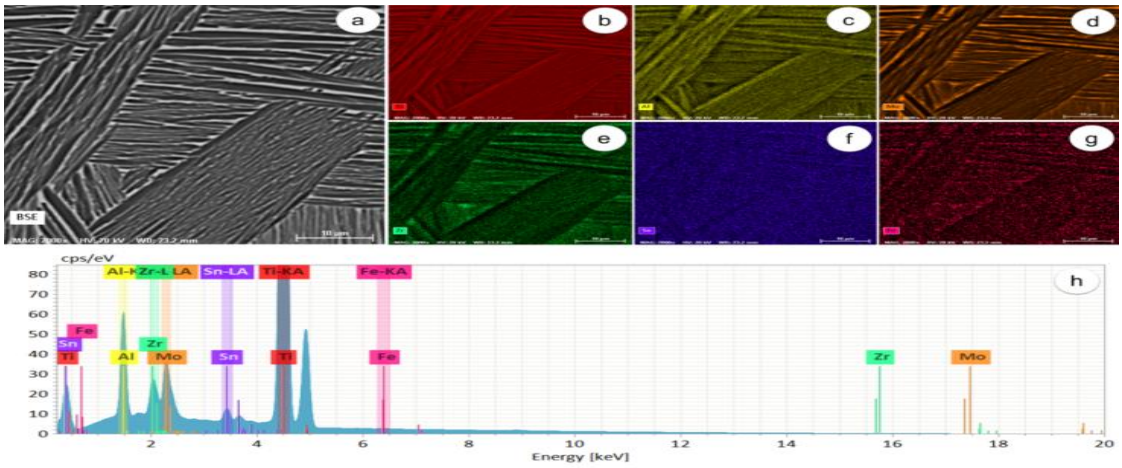

Figure 6. Alloying elements dispersion within the sample V (hot-deformed at 900°C and normalized at 950°C); a) high magnification BSE image of sample V microstructure; b) Ti dispersion; c) Al dispersion; d) Mo dispersion; e) Zr dispersion; f) Sn dispersion; g) Fe dispersion; h) EDS spectra of sample V.

Table 3. Statistical data on the chemical composition of all samples

Samples	Element	Line	Mass [% wt]	Mass [% at]	Absolute error [%]	Relative error [%]
As-cast alloy (Sample I)	Titanium (Ti)	K-Serie	83.45	84.54	2.36	2.79
	Aluminium (Al)	K-Serie	5.50	9.89	0.29	5.22
	Molybdenum (Mo)	L-Serie	5.96	3.02	0.24	3.95
	Zirconium (Zr)	L-Serie	3.60	1.91	0.16	4.47
	Tin (Sn)	L-Serie	1.43	0.58	0.07	4.67
	Iron (Fe)	K-Serie	0.06	0.05	0.03	44.98
	Sum		100	100		
Sample II	Titanium (Ti)	K-Serie	83.12	83.91	2.33	2.79
	Aluminium (Al)	K-Serie	5.93	10.62	0.31	5.19
	Molybdenum (Mo)	L-Serie	5.55	2.8	0.22	3.98
	Zirconium (Zr)	L-Serie	3.77	2	0.17	4.45
	Tin (Sn)	L-Serie	1.61	0.65	0.07	4.48
	Iron (Fe)	K-Serie	0.02	0.02	0	2.7
	Sum		100	100		
Sample III	Titanium (Ti)	K-Serie	83.23	84.32	2.31	2.79
	Aluminium (Al)	K-Serie	5.61	10.09	0.29	5.22
	Molybdenum (Mo)	L-Serie	5.97	3.02	0.23	3.96
	Zirconium (Zr)	L-Serie	3.62	1.92	0.16	4.48
	Tin (Sn)	L-Serie	1.54	0.63	0.07	4.57
	Iron (Fe)	K-Serie	0.02	0.02	0	2.71
	Sum		100	100		
Sample IV	Titanium (Ti)	K-Serie	83.3	84.01	2.33	2.79
	Aluminium (Al)	K-Serie	5.94	10.63	0.31	5.19
	Molybdenum (Mo)	L-Serie	5.32	2.68	0.21	4.01
	Zirconium (Zr)	L-Serie	3.76	1.99	0.17	4.45
	Tin (Sn)	L-Serie	1.67	0.68	0.07	4.43
	Iron (Fe)	K-Serie	0.02	0.02	0	2.71
	Sum		100	100		
Sample V	Titanium (Ti)	K-Serie	82.92	83.85	2.35	2.79
	Aluminium (Al)	K-Serie	5.89	10.56	0.31	5.19

Molybdenum (Mo)	L-Serie	5.68	2.87	0.23	3.97
Zirconium (Zr)	L-Serie	3.72	1.97	0.17	4.45
Tin (Sn)	L-Serie	1.76	0.72	0.08	4.34
Iron (Fe)	K-Serie	0.03	0.03	0	2.68
Sum		100	100		

3.2. Metallographic Analysis

The results of SEM and OM microstructures of the Ti-6246 as-cast alloy (sample I) with different magnification factors are shown in Figure 7. It can observe that Figure 7c have a higher magnification factor and the microstructure of this sample contains two phases. The α phase that refers to the darker color and the β phase which indicates to the brighter color. The structure of as-cast alloy was alternate α-lamellar morphology in diverse orientations with a β-phase matrix to forms eventually α + β lamellar. As well the volume fraction of α phase is higher than the β phase volume fraction (Figures 7a and 7b). Moreover, Figure 7d presents the results of OM microstructure of the Ti-6246 as-cast alloy (sample I). As described above, the microstructure of OM has both phases but in contrast with SEM microstructures, where α phase which indicates to the brighter color and β phase that refers to the darker color. Furthermore, the microstructure of OM has been determined as α + β lamellar that crossed with each other aligned similarly in SEM microstructures. One can see in Figure 7d, the form of the grain is quite large and the high content of α phase between the grains boundaries.

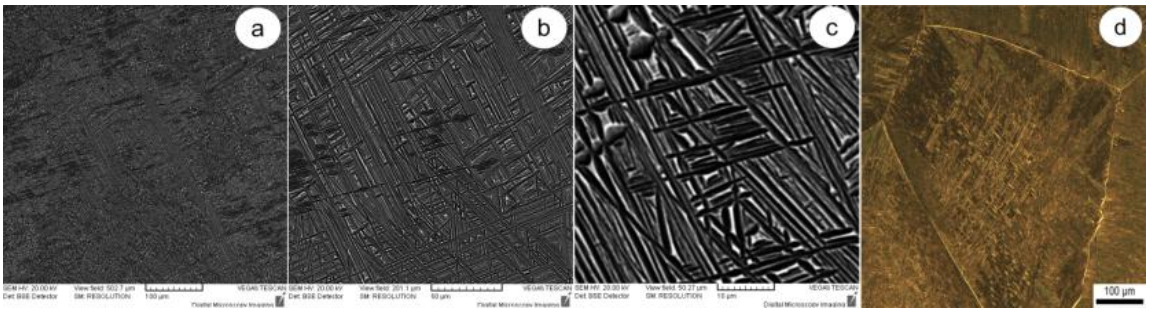

Figure 7. SEM and OM microstructures of the as-cast sample (Sample I).

The microstructures have been examined by SEM and OM in sample II that carried out the hot plastic deformation at 800°C with time duration of 15 minutes as depicted in Figure 8. The results revealed that there is an important alter/change in the microstructure that consists of a large quantity of α phase with a heterogeneous distribution of thick α lamellar morphology along with a much amount of β phase matrix. Moreover, it was observed that inside the β phase matrix itself there are precipitations of the α lamellar colonies (Figure 8c). Furthermore, the slow cooling procedure leads to increase in the thickness of individual lamellae and various sizes of α lamellar dispersed in different orientations as shown in Figures 8a and 8b. Whereas in Figure 8d, there is an obvious elongation take place for the grains in the middle of the sample in different orientations. It was found that the microstructure comprises a mixture of α and β phases.

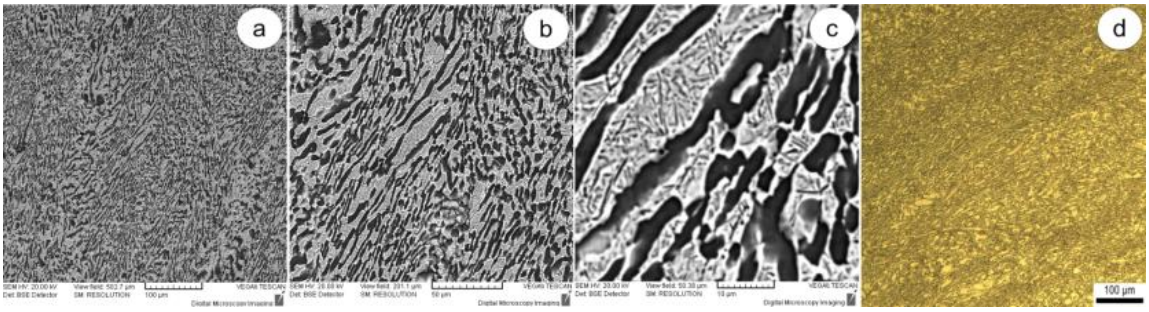

Figure 8. SEM and OM microstructures of sample II during the hot-deformed process at 800°C.

In the micrographs shown in Figure 9, the results of the microstructures of sample III were captured through SEM and OM. The hot deformation process and normalized heat treatment were conducted at temperatures of 800°C and 950°C one by one. Nevertheless, once the sample is heated again at a temperature slightly above the Tβ which led to recrystallization occurrence in the microstructure of both phases and change/alter the structure to the α + β lamellar aligned similarly as in the as-cast material. One can see in Figure 9b, the formation of slightly large α grains size as a result of adequately slow cooling and inside these α grains themselves there are α + β lamellar colonies. While Figure 9c displays the appearance of small grains that represent the site of junctions between the other bigger grains sizes as a result of the low temperature. The cooling rate used in the alloy is the essential determiner to the nature of these α colonies textures. The α grains are large/coarse when the cooling procedure enough slowly. Thereby, these colonies can grow to be quite long (hundreds of microns) [29]. Once seeing Figure 9d, the microstructure was almost comparable to the parent sample (small α + β lamellar colonies), apparently, it has realized the prosperity of the small grains in comparison with the parent sample.

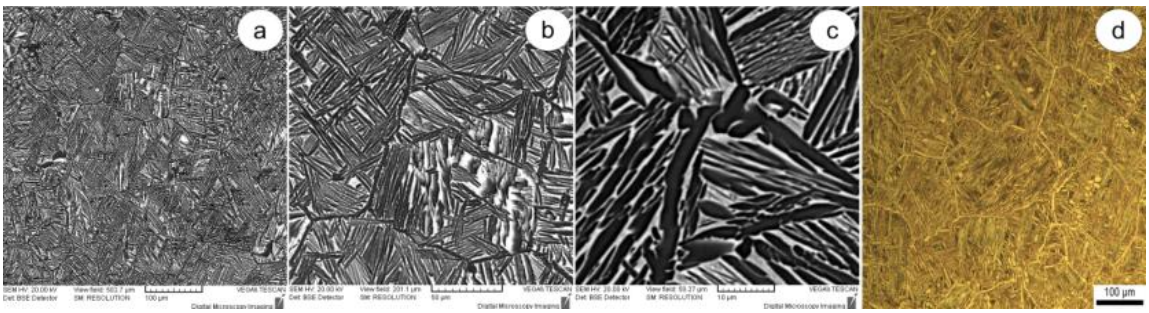

Figure 9. SEM and OM microstructures of sample III during the hot-deformed process at 800°C and normalized heat treatment process at 950°C.

The microstructures of sample IV that were analyzed using SEM and OM are shown in Figure 10. The hot plastic deformation process has been applied at 900°C during the time duration of 15 minutes. It was detected that the microstructure comprises of also a heterogeneous arrangement of α phase with morphology looks like crooked α lamellar into β phase matrix. However, it can be seen in Figures 10a and 10b that the effect of increasing temperature limits the expansion of these α plates and makes them less intensive and propagation. The significant difference in the microstructure was in the β phase where became a full massive amount of β phase (i.e. there are no α lamellar colonies into β phase itself as illustrated in Figure 10c) in comparison with the sample that carried out the hot deformation at 800°C (Figure 8c). While in Figure 10d the same procedure appears which previously discussed in Figure 9d. But manifests the microstructure is more explicit at mid-sample. It produces much more α and β phases ranges as a comparison to the lower temperature that represented in Figure 8d.

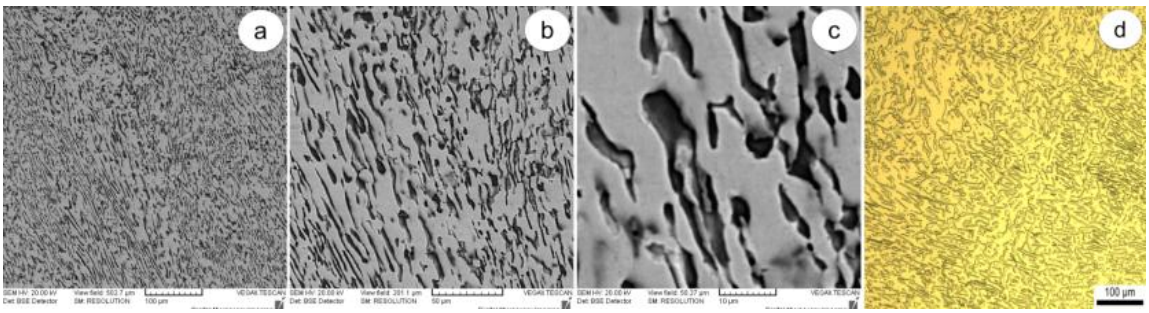

Figure 10. SEM and OM microstructures of sample IV during the hot-deformed process at 900°C.

The micrographs have been explored during SEM and OM; the outcomes of the microstructures for sample V are shown in Figure 11. The hot deformation process and normalized heat treatment were performed at temperatures of 900°C and 950°C respectively. As described earlier when the sample is

heated once again the structure is recrystallized to form somewhat large grains size as seen in Figures 11a and 11b. Despite the size of the grains depends on the cooling rate conditions, but the time duration for the heating process plays an important role in controlling grains sizes. Therefore, the cooling rate that used was slow enough to forms large grain size. In contrast, the time duration was not enough to generate a very fine grain size. Figures 11b and 11c can explain the change that takes place in the microstructure which consisting of a big content of both phases with a morphology α + β acicular lamellar, where α phase begins with growth and nucleation to pinned from the grains boundaries and propagate continuously inside the grains. Whilst in Figure 11d the microstructure was contained a large of α + β lamellar colonies along with large grains size conversely to the grains that appear in sample III (Figure 9d).

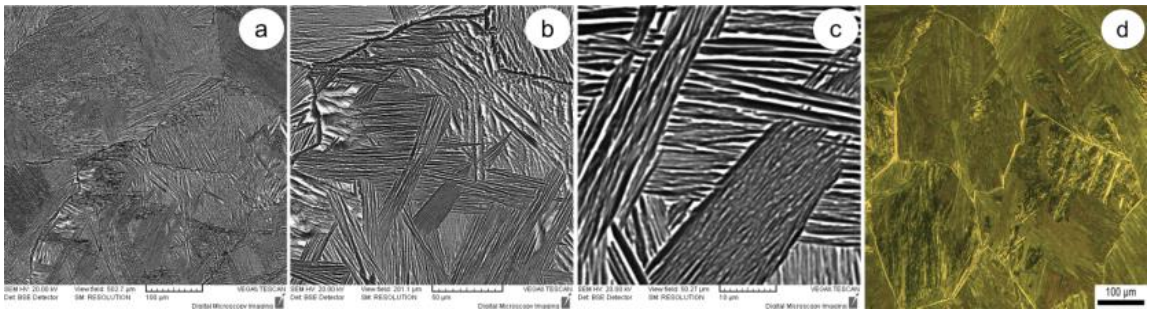

Figure 11. SEM and OM microstructures of sample V during the hot-deformed process at 900°C and normalized heat treatment process at 950°C.

4. Conclusions

The principal purpose of this paper is to detect the effect of the microstructures features (the grains size, grain boundaries, the thickness of lamellar, and lamellar colonies) that were exposed to a combination of hot mechanical work and heat treatment in the α + β and β field range sequentially. It was concluded the most significant variable is the temperature which has a strong effect on the microstructure evolution, although the temperatures were less than the temperature of recrystallization for the deformed samples. However, it had provided differently morphologies in the microstructure analysed by SEM and OM devices in comparison with the other thermo-mechanical variables such as time duration and cooling rate. Otherwise, the time duration (15 minutes) for both deformed samples was had no great role in influencing the microstructures like the temperature. Moreover, the slow cooling rate makes the morphology of α + β lamellar thicker as compared to the parent sample.

For the deformed and normalized samples that examined in the SEM and OM devices, it was concluded that all heat treatment variables (temperature, time duration and cooling rate) have an important effect on the microstructures features. Where the temperature became slightly above the recrystallization temperature along with the cooling rate which was sufficiently slowly led to generate in somewhat large grains due to the time duration is not long enough (30 minutes), but it small than the as-cast alloy. From the mechanical viewpoint, the smaller grains are favoured for the mechanical characteristics. Therefore, the microstructures features were enhanced as compared to the as-cast alloy and deformed samples. As well it was concluded that the first case of the normalization process applied to the third sample produced small grains as junction zones between the large grains because the temperature was not high compared with the second case of the normalization process had performed on the fifth sample, hence, sample five had created a finer α + β lamellar textures morphology than sample three.

References

[1]. Boyer R R 1996 *Mater. Sci. Eng.* A **213** 103-114.
[2]. Gorynin I V 1999 *Mater. Sci. Eng.* A **263** 112-116.
[3]. Inagaki I, Takechi T, Shirai Y and Ariyasu N 2014 *NSSMC.* **106** 22-27.
[4]. Boyer R, Collings E W and Welsch G 1994 *Materials Properties Handbook: Titanium Alloys* (USA: ASM International) p 1169.

[5]. Ezugwu E O and Wang Z M 1997 *J. Mater. Process. Technol*. **68** 262-274.
[6]. Joshi V A 2006 *Titanium Alloys: an Atlas of Structures and Fracture Features* (USA: Taylor & Francis Group) p 247.
[7]. Soo S L, Antar M T, Aspinwall D K, Sage C, Cuttell M, Perez R, Pereze R and Winn A J 2013 *Procedia CIRP*. **6** 215-219.
[8]. Chapman T P, Chater R J, Saunders E A, Walkerc A M, Lindleya T C and Dye D 2015 *Corros. Sci.* **96** 87-101.
[9]. Luo J, Gao J, Li L and Li M Q 2016 *J. Alloys Compd.* **667** 44-52.
[10]. Pretorius C j, Soo S L, Aspinwall D K, Harden P M, M'Saoubi R and Mantle A L 2015 *CIRP Ann. Manuf. Technol*. **46** 109-112.
[11]. Pederson R, Niklasson F, Skystedt F and Warren R 2012 *Mater. Sci. Eng.* A **552** 555-565.
[12]. Lütjering G and Williams J C 2007 *Titanium: Engineering Materials and Processes Series* (Berlin Heidelberg /Germany: Springer-Verlag) p 449.
[13]. Gammon L M, Briggs R D, Packard J M, Batson K W, Boyer R and Domby C W 2004 *Metallography and Microstructures of Titanium and Its Alloys* vol 9, ed G F V Voort (USA: ASM International Handbook) pp 899-917.
[14]. Alluaibi M H, Rusea A, Cojocaru V D 2018 *U.P.B. Sci. Bull.* B **80** 245-258.
[15]. Fujii H 1998 *Mater. Sci. Eng.* A **243** 103-108.
[16]. Filip R, Kubiak K, Ziaja W and Sieniawski J 2003 *J. Mater. Process. Technol*. **133** 84-89.
[17]. Wang K X, Zeng W D, Zhao Y Q, Lai Y J, Zhang X M and Zhou Y G 2011 *Mater. Sci. Technol*. **27** 21-28.
[18]. Xu Y, Lu Y, Sisson R D and Jr 2015 *Proc. of the 28th ASM Heat Treating Society Conference* (Detroit-Michigan/USA: ASM International) pp 358-364.
[19]. Froes F H 2016 *Reference Module in Mater. Sci. Mater. Eng*. 1-7.
[20]. Boyer H E, and Gall T L 1992 *Properties and Selection: Nonferrous Alloys and Special-Purpose Materials* vol 2, ed L Robert et al. (USA: ASM International Handbook) p 3470.
[21]. Semiatin S L, Seetharaman V and Weiss I 1997 *JOM*. 33-68.
[22]. Donachie M J 2000 *Titanium: A Technical Guide* (USA: ASM International) p 216.
[23]. Weiss I and Semiatin S L 1998 *Mater. Sci. Eng.* A **243** 46-65.
[24]. Weiss I and Semiatin S L 1999 *Mater. Sci. Eng.* A **263** 243-256.
[25]. Bell T and Dong H 2000 *Proc. of the 12th Int. Conf. on Titanium (IFHTSE)* vol 2 (Australia: Melbourne/IWT Bremen) pp 1-10.
[26]. Szczepanski C J, Jha S K, Larsen J M and Jones J W 2008 *JOM.* **39** 2841-2851.
[27]. Froes F H 2015 *Titanium Physical Metallurgy Processing and Applications* (USA: ASM International) p 417.
[28]. Banerjee S and Muchopadhyay P 2007 *Phase Transformations: Examples from Titanium and Zirconium Alloys* (UK: Elsevier) p 840.
[29]. Liu A F 2005 *Mechanics and Mechanisms of Fracture: An Introduction* (USA: ASM International) p 467.